This MICCAI paper is the Open Access version, provided by the MICCAI Society. It is identical to the accepted version, except for the format and this watermark; the final published version is available on SpringerLink.

Supplementary material to the manuscript "CLEAR: Complex Learned Explicit Analytical Regularization for Ultra-Accelerated 4D Flow CMR Reconstruction"

German Shâma Wache and Sebastian Neumayer
Chemnitz University of Technology, Germany
{german-shama.wache,sebastian.neumayer}@mathematik.tu-chemnitz.de

S.1 Illustration of the regularizer architecture

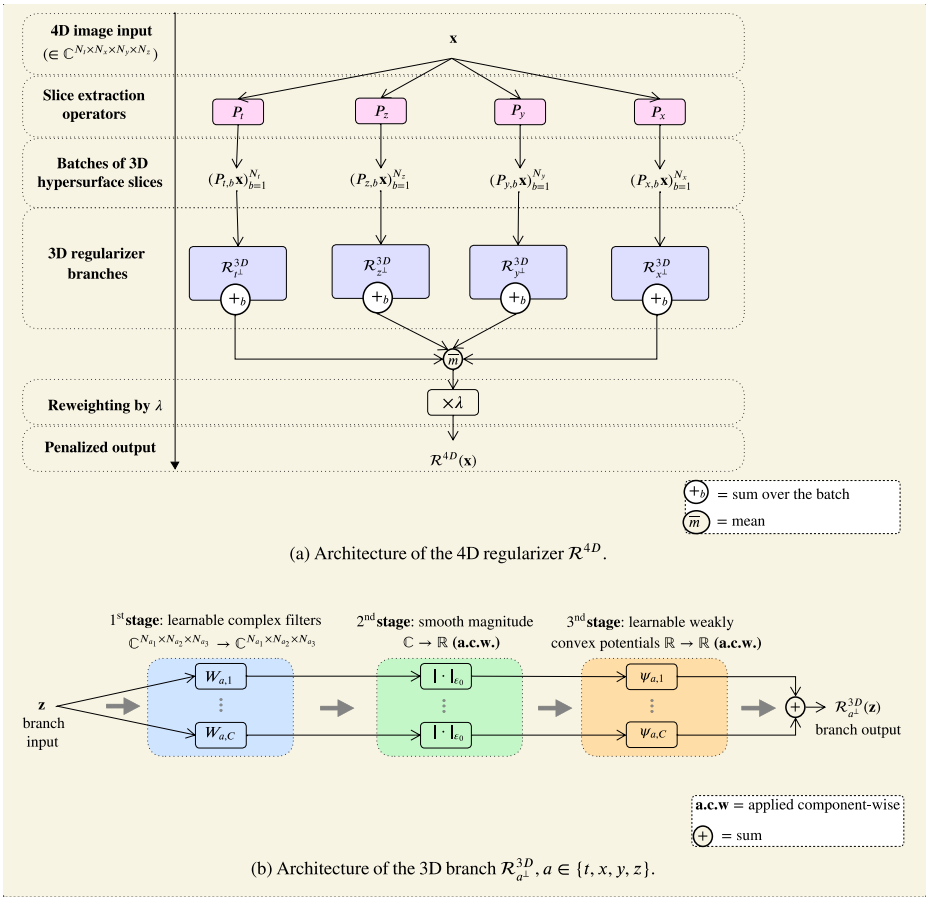

(a) Architecture of the 4D regularizer $\mathcal{R}^{4D}$.

(b) Architecture of the 3D branch $\mathcal{R}^{3D}_{a^\perp}$, $a \in \{t, x, y, z\}$.

Fig. S1. Illustration of the proposed regularizer (CLEAR) architecture.

S.2 Jacobian-free backpropagation training details

Let θ be the collection of all learnable parameters, and write $\mathcal{R}^{4D}_{\theta(R)}$ to make the dependence on the acceleration factor R explicit. An $R\times$-accelerated k-space $\mathbf{y} \in \mathbb{C}^{N_t \times N_c \times N_x \times N_y \times N_z}$ is reconstructed as $\widehat{\mathbf{x}} \in \mathbb{C}^{N_t \times N_x \times N_y \times N_z}$ according to

$$\widehat{\mathbf{x}}(\mathbf{y}, \theta) = \arg\min_{\mathbf{x}} \frac{1}{2}\|\mathbf{M}_R \mathcal{F}\mathbf{S}\mathbf{x} - \mathbf{y}\|_2^2 + \mathcal{R}^{4D}_{\theta(R)}(\mathbf{x}), \tag{S1}$$

which we solve using the nmAPG solver.

At the Adam optimizer step j, let $\{(\mathbf{x}^{j,b}, \mathbf{y}^{j,b})\}_{b\in\mathcal{B}}$ be the training batch, where $\mathbf{y}^{j,b}$ is $R^{j,b}\times$-accelerated. A direct parameter update would require backpropagating through $\sum_{b\in\mathcal{B}} \|\widehat{\mathbf{x}}(\mathbf{y}^{j,b}, \theta) - \mathbf{x}^{j,b}\|_2^2$, where $\widehat{\mathbf{x}}(\mathbf{y}^{j,b}, \theta)$ is obtained by solving the lower-level variational problem (S1) with nmAPG. Instead, we detach the nmAPG reconstruction $\widehat{\mathbf{x}}(\mathbf{y}^{j,b}, \theta)$ from the computational graph and take one additional gradient step:

$$\widetilde{\mathbf{x}}(y^{j,b}, \theta) = \widehat{\mathbf{x}}(y^{j,b}, \theta) - \frac{1}{L_{j,b}} \nabla_{\mathbf{x}} \left[\frac{1}{2}\|\mathbf{M}_{R^{j,b}} \mathcal{F}\mathbf{S}\mathbf{x} - \mathbf{y}^{j,b}\|_2^2 + \mathcal{R}^{4D}_{\theta(R_{j,b})}(\mathbf{x}) \right]_{\mathbf{x}=\widehat{\mathbf{x}}(y^{j,b},\theta)}. \tag{S2}$$

Here, $L_{j,b}$ is the local Lipschitz of the variational objective. The parameters θ are then updated by backpropagating only through this last step, using $\sum_{b\in\mathcal{B}} \|\widetilde{\mathbf{x}}(\mathbf{y}^{j,b}, \theta) - \mathbf{x}^{j,b}\|_2^2$.

S.3 Reported metrics

Let $\mathbf{x}_0$ and $\mathbf{x}_0^*$ denote the reconstructed and reference magnitude images of the reference encoding, and let $\widehat{\mathbf{v}}$ and $\mathbf{v}^*$ denote the reconstructed and reference velocity fields. We reported

$$\mathrm{nRMSE}(\mathbf{x}_0, \mathbf{x}_0^*) = \sqrt{\sum_i \frac{(x_{0,i} - x^*_{0,i})^2}{N \max_j (x^*_{0,j})^2}},$$

$$\mathrm{RelErr}(\widehat{\mathbf{v}}, \mathbf{v}^*) = \frac{\big\| |\widehat{\mathbf{v}}| - |\mathbf{v}^*| \big\|_2}{\big\| |\mathbf{v}^*| \big\|_2},$$

$$\mathrm{AngErr}(\widehat{\mathbf{v}}, \mathbf{v}^*) = \arccos\left(\frac{\langle \widehat{\mathbf{v}}, \mathbf{v}^* \rangle}{\|\widehat{\mathbf{v}}\|_2 \|\mathbf{v}^*\|_2} \right).$$

Additionally, we reported the structural similarity index (SSIM) on the reconstructed reference-encoding magnitude images.

S.4 Tuning details for LLR

The LLR baseline promotes low-rank structure in local patch matrices. Given a 4D image $\mathbf{x}$, the LLR penalty is

$$\mathcal{R}_{\mathrm{LLR}}(\mathbf{x}) = \lambda_{\mathrm{LLR}} \sum_{i=1}^{N_{\mathrm{ptch}}} \|\mathbf{T}_i \mathbf{x}\|_*,$$

where $\mathbf{T}_i$ extracts the i-th local $p \times p \times p$ patch from all N_t cardiac frames, N_{ptch} is the number of patches, and $\|\cdot\|_*$ denotes the nuclear norm. The corresponding convex optimization problem is solved with FISTA and stopped when the relative change between consecutive iterates falls below 10^{-3}, after which the RelErr remains unchanged. We tuned λ_{LLR} separately for each acceleration factor present in the evaluation data ($R = 10, 20, 30, 40, 50$). This was done on the training data by grid search to minimize RelErr, obtaining $\lambda_{\text{LLR}} = 0.4, 0.6, 0.6, 0.8, 0.8$ for $R = 10, 20, 30, 40, 50$, respectively.

S.5 CLEAR's learned components (full visualization)

In each 3D branch, the per-filter potentials are just a rescaling of the base potential and keep the same shape. We therefore only present the base potential in each branch.

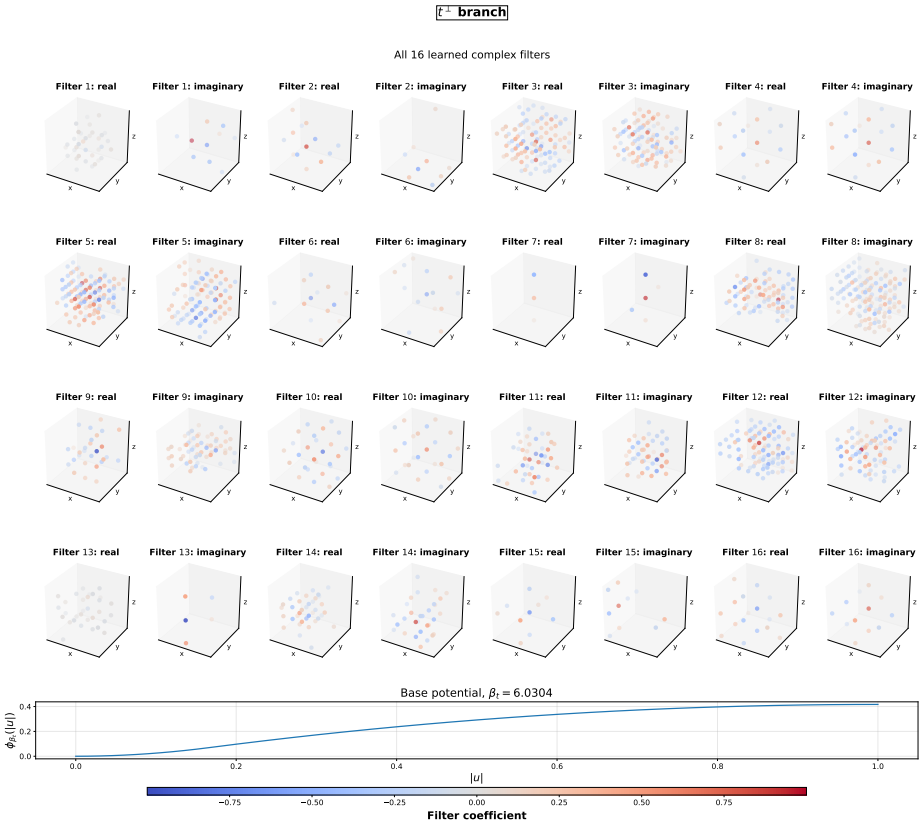

Fig. S2. CLEAR's learned components (complex filters and base potential) in the $t^{\perp}$ 3D branch. Only filter coefficients with magnitudes larger than 15% of the maximum magnitude filter coefficient are displayed for clarity.

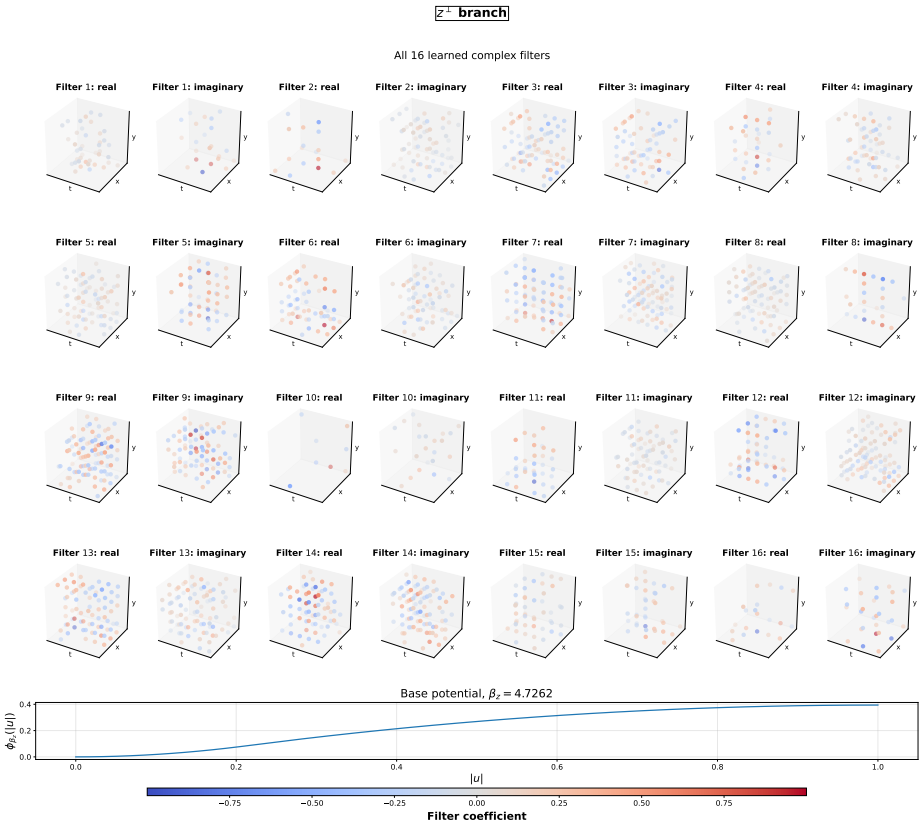

Fig. S3. CLEAR's learned components (complex filters and base potential) in the $z^{\perp}$ 3D branch. Only filter coefficients with magnitudes larger than 15% of the maximum magnitude filter coefficient are displayed for clarity.

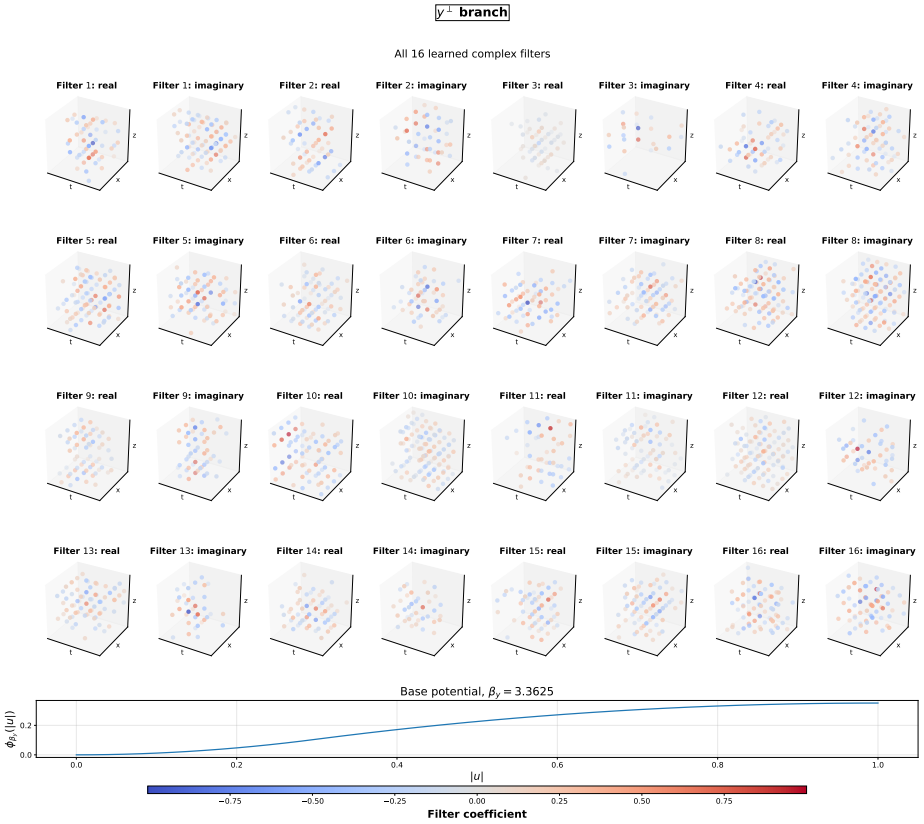

Fig. S4. CLEAR's learned components (complex filters and base potential) in the $y^{\perp}$ 3D branch. Only filter coefficients with magnitudes larger than 15% of the maximum magnitude filter coefficient are displayed for clarity.

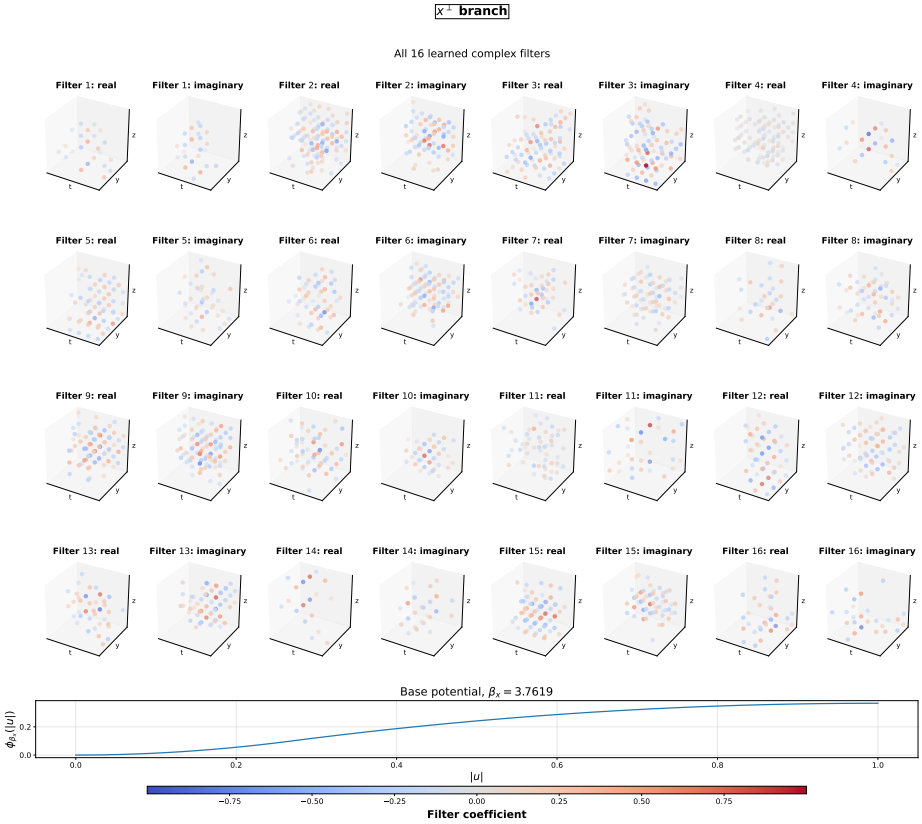

Fig. S5. CLEAR's learned components (complex filters and base potential) in the $x^{\perp}$ 3D branch. Only filter coefficients with magnitudes larger than 15% of the maximum magnitude filter coefficient are displayed for clarity.